A New Approach to the Study of Protein−Protein Interaction by FTIR: Complex Formation between Cytochrome P450BM-3 Heme Domain and FMN Reductase Domain†

Andrei Kariakin,‡ Dimitri Davydov,§ Julian A. Peterson,|| and Christiane Jung*,‡

Max-Delbrück-Center for Molecular Medicine, Protein Dynamics Laboratory, 13125 Berlin, Germany, Department of Pharmacology & Toxicology, University of Texas Medical Branch at Galveston, Galveston, Texas 77555-1031, and Department of Biochemistry, University of Texas Southwestern Medical Center, Dallas, Texas 75235-9038

Received June 5, 2002; Revised Manuscript Received September 20, 2002

ABSTRACT: We describe a new approach to the study of protein−protein interaction using Fourier transform infrared spectroscopy (FTIR). This approach is based on the combination of FTIR technique with both protein titration experiments and the principal component analysis (factor analysis) of the IR absorption spectra in the 1500−1800 cm^{-1} region for the protein mixtures. We have applied this approach to the interaction of the heme domain with the FMN domain of bacterial monooxygenase cytochrome P450BM-3 (CYP102A1). The analysis reveals that the first principal component reflects the protein−protein complex formation because the loading factors show a clear systematic dependence on the concentration of the heme domain according to a titration curve with a dissociation constant of ∼5 μM. The spectrum of the first principal component has been assigned to structural changes in the secondary structure (increase of β-sheet and α-helix and decrease of turn structures), amino acid side chains (protonation of aspartate and C-terminal COO group), and deprotonation of a propionic acid COOD group in the heme.

The interaction between different proteins is a fundamental phenomenon in biological systems. It plays a pivotal role in the regulation of the protein assemblies, being at the same time a prerequisite for intermolecular electron transfer in redox cascades. In the former case, the interfaces of interacting proteins are thought to involve superficial recognition sites, whose interactions are essentially of electrostatic nature (*1*, *2*). The interactions between proteins may induce their conformational changes, which in addition to structural transitions in the docking regions might involve more global rearrangements of the protein conformation. The best visualization of protein−protein interaction might be obtained by a comparison of the crystal structures of single proteins with that of the protein−protein complex (*1*, *3*). It is generally assumed that the crystal structure adequately reflects the conformation of the protein in solution. In many cases, however, it appears impossible to crystallize the proteins and their complexes, and other techniques are required for the analysis of protein−protein interactions. Here we apply Fourier transform infrared spectroscopy (FTIR) combined with the principal component analysis (PCA) to reveal the association-induced changes in the protein structures. This represents a new approach to the studies of protein−protein interactions.

The secondary structure of proteins is reflected in the amide I absorption band that predominantly originates from the stretching vibration of the peptide backbone C═O groups involved in various hydrogen bonding patterns (*4*−*6*). Amino acid side chain infrared absorption may reflect formation or changes of salt links (*7*−*9*). Changes in the infrared absorption of the N−H bending in the peptide backbone (amide II band) can be used to study folding and unfolding behavior (*10*, *11*). Furthermore, local spectroscopic probes, such as the stretching mode vibration bands of the heme iron ligands (i.e., CO, NO) in heme proteins (*6*), might be successfully employed to complete the analysis of the structural changes induced by protein−protein interactions. To use the advantages of FTIR one has to solve, however, two major methodological problems: (i) to assign each particular spectral marker of the interactions to a specific structural rearrangement in the proteins and (ii) to establish criteria to distinguish between the spectral markers of the protein−protein interactions and the unspecific signals originating from noninteracting protein molecules, as well as from the molecules of solvent and other components of the sample solution. Problem i can be partially solved by uniform

† This study was supported by the Deutsche Forschungsgemeinschaft Grant INK 16/B1-1 (to C.J.), NIH Grant GM50858-06 (to J.A.P.), and INTAS Grant 96-1343 (to C.J. and D.R.D.).

* Corresponding author. Address: Max-Delbrück-Center for Molecular Medicine, Protein Dynamics Laboratory, Robert-Rössle-Strasse 10, D-13125 Berlin, Germany. Phone: +49-30-94063370. Fax: +49−30−94063329. E-mail: cjung@mdc-berlin.de.

‡ Max-Delbrück-Center for Molecular Medicine.

§ University of Texas Medical Branch at Galveston.

|| University of Texas Southwestern Medical Center.

[1] Abbreviations: FTIR, Fourier transform infrared spectroscopy; BMP, the substrate-free heme protein domain of monooxygenase P450 μ_B-3 from *Bacillus megaterium*, CYP102; FMND, the FMN-containing domain of P450 μ_B-3; FMN, flavin mononucleotide; FAD, flavin adenine dinucleotide; PCA, principal component analysis; HEPES, *N*-(2-Hydroxyethyl)piperazine-*N*′-(2-ethanesulfonic acid); CPR, NADPH-cytochrome P450 reductase.

10.1021/bi0262505 CCC: $22.00
Published on Web 10/25/2002

^{13}C- and ^{15}N-isotope labeling of one of the interacting proteins. The amide I band of the labeled protein is shifted by more than 55 cm^{-1} to lower frequencies (*12*, *13*) and therefore separates from the normally overlapping amide I bands of the interacting proteins. The separated amide I bands allow therefore the assignment of the observed spectral changes to the specific protein. However, this approach excludes the possibility of analyzing the spectral changes in the amino acid side chains due to overlapping of the shifted amide I band of the labeled protein with the spectral region of the side chains (e.g., aspartates and glutamates) of the unlabeled protein. Site-directed mutagenesis in one of the interacting proteins may also be helpful in the assignment of the structural changes due to protein−protein interaction. However, the effect of one amino acid replacement on the amide I absorption band of the protein is certainly marginal. Such replacement may cause considerable spectral changes only if the side chain absorption bands (i.e., those of aspartates or glutamates) are affected.

A powerful approach to resolve problem ii might be provided by factor analysis (*14*−*16*) employed to analyze a series of FTIR spectra obtained at various concentrations of interacting proteins. This approach, which is referred to here as principal component analysis (PCA), is often formalized in terms of the singular value decomposition (SVD) algorithm (*16*, *17*). It is applicable to resolve overlapping spectral transitions in complex systems. PCA is widely used to analyze two-dimensional data arrays (i.e., series of spectra obtained for changing reagent concentration, time, temperature, pressure, etc.) in various spectroscopic (*14*, *17*−*19*) and chromatographic (*15*) techniques.

Factor analysis in FTIR studies has been applied in pattern recognition-related approaches, such as determination of the concentrations of structurally diverse compounds in their mixtures (*20*) or for determination of the secondary structure composition of pure proteins from their FTIR spectra (*21*, *22*). In the latter case, a large set of FTIR spectra of different proteins with known secondary structure forming the calibration database is subjected to a factor analysis procedure, and the resulting principal component spectra (eigenvectors) and their corresponding loading factors are used to determine the percentage of the specific secondary structure elements in the protein under analysis (*21*, *22*). An attempt to use PCA to analyze structural transitions in proteins was recently made by Stelea and coauthors in their work on thermal unfolding of ribonuclease A (*23*). In the present paper, we present the first example of the application of principal component analysis to resolve the association-induced structural changes in proteins by FTIR. Here we describe the general algorithm for the pretreatment of FTIR spectra and subsequent PCA procedure, as well as the strategy on how to assign the PCA-resolved principal components in FTIR spectra to the specific structural changes.

As the object for this study, we have chosen the protein−protein interaction of constituents in the cytochrome P450 monooxygenase system. Cytochromes P450 represent a large superfamily of heme thiolate proteins that catalyze the conversion of a great variety of chemically diverse compounds by insertion of an oxygen atom into an inert C−H bond (*24*). The required activation of molecular oxygen is achieved by transfer of two electrons from NAD(P)H via redox proteins to the terminal cytochrome P450. There are two main classes of monooxygenases that differ in the nature of redox proteins involved in the electron transfer to P450. In the first class, in which cytochrome P450cam (CYP101) from *Pseudomonas putida* is the typical example, the electron-transfer proceeds from NADH to a flavin reductase and from there to the iron−sulfur protein putidaredoxin (Pdx). Pdx interacts with P450cam and transfers the electrons to the P450 heme (*25*). In the second class the electron-supplying chain is represented by a single protein—NADPH-cytochrome P450 reductase (CPR), which contains two flavins—FAD and FMN as redox centers. CPR directly interacts with cytochrome P450 to transfer the electrons from NADPH via FAD to FMN and then to the heme iron of cytochrome P450. Although the reductase and the P450 proteins are usually represented by two separate polypeptide chains, as is seen in the microsomal monooxygenase systems, they may also form a single chimerical molecule containing both the cytochrome P450-like heme domain and the reductase-like flavin-containing domain (reductase domain). The P450BM-3 monooxygenase (CYP102) from *Bacillus megaterium* is an example of the latter case. The reductase domain itself consists of an FAD subdomain and an FMN subdomain where the FMN subdomain is the redox partner for the heme domain (*26*). The crystal structure of the single heme domain protein of CYP102 (BMP) has been reported previously (*27*) as well as the structure of its complex with a substrate (*28*), both at high resolution. The crystal structure of the complex of the CYP102 reductase FMN subdomain (FMND) with BMP has been recently reported as well (*3*).

In this paper we report the first FTIR analysis of the interaction of the FMN domain with BMP. We demonstrate that the interaction of these proteins induces important changes in the secondary structure in both of them. Notably, these changes are not restricted to the surface regions but apparently also involve rearrangements within the protein core. The FMND−BMP interaction is used here to demonstrate the advantages of the combination of FTIR spectroscopy with the principal component analysis in the studies of protein−protein interaction-induced structural transitions in proteins. In a separate paper, we present a FTIR study on the Pdx-P450cam system.

MATERIALS AND METHODS

Proteins and Chemicals. The purification of the substrate-free heme protein domain of P450BM-3 (BMP), from *E. coli* clones containing a plasmid encoding this protein, was described previously (*29*). The purification of the FMN-containing domain of P450BM-3 (FMND) is described elsewhere (*26*, *30*). Deuterium oxide and HEPES buffer were obtained from SIGMA.

Protein FTIR Sample Preparation. A small aliquot (100−300 μL) of the concentrated protein (400−600 μM) was extensively dialyzed against deuterated HEPES−K^+ buffer, 10 mM, pD 7.4 (D-HEPES), on a membrane of Slide-A-Lyser Mini Dialysis Units 10,000 MWCO (PIERCE, USA) at +4 °C. Deuterated BMP and FMND solutions were used either to measure the FTIR spectra of the pure proteins (standard spectra) or to compose the mixtures of the proteins with different concentrations. These mixture samples were frozen and kept at −20 °C until further use. All manipulations with the protein samples were performed in a glovebox

under purging with dried nitrogen to protect the samples against deuterium/proton exchange originating from air−water vapor.

FTIR Spectra Measurements. Infrared spectra were recorded at 25 °C using the Bruker IFS 66 Fourier transform infrared spectrometer equipped with a liquid nitrogen-cooled MCT detector. The protein solution at room temperature was placed in a custom-made demountable cell with CaF_2 windows separated by a Teflon spacer having a thickness of 23.61 ± 0.38 μm. To compensate for D-HEPES absorption, the buffer solution was placed in the same cell and used as reference.

The spectral resolution was set to 2 cm^{-1} in a double-sided/forward−backward acquisition mode. Fourier transformations of up to 3000 co-added interferograms of both sample and reference were performed with the Blackman−Harris four-term apodization function and a zero-filling factor of 2 in the region 800−4000 cm^{-1}. For each sample several FTIR absorption spectra were collected. Three to five measurements were averaged to obtain the final FTIR absorption spectrum of the sample. Residual water vapor absorption was interactively subtracted from the sample spectra.

Primary infrared spectra treatment. A two-step procedure was used for infrared spectra treatment. In the first step (i), the spectra of the pure proteins were measured and analyzed to get standard spectra. The measurement and treatment of the mixture spectra using the standard spectra followed as the second step (ii). Because the absorption changes due to the protein complex formation were expected to be very small (in the optical density range of 10^{-4}) as compared to the absolute protein absorption (0.015−0.1), the contribution of noise, baseline drift, and protein sampling errors might not have been negligible. Therefore, all spectra had to be corrected to diminish these errors prior to the PCA analysis.

(i) Spectra of the Pure Proteins (Standard Spectra). We recorded a series of FTIR spectra of the pure proteins taken at various concentrations within the range used in the titration experiments. These series, recorded in the spectral range of 1300−1800 cm^{-1}, were then subjected to the PCA treatment described below. The spectrum of the first principal component (e.g., the first eigenvector) was then treated as a spectral standard of the pure protein. This procedure allows extracting the changes caused by the increase in the protein concentration diminishing the influence of the baseline drift and improving the signal-to-noise ratio. Great care was taken to prepare the protein samples and the reference buffer solutions under tightly controlled conditions in a glovebox. Nevertheless, a D/H exchange could not be completely avoided, as was seen by a variable increase in the absorption around 1450 cm^{-1} that resulted from the HOD bending vibration, which overlaps with the amide II′ of the protein in D_2O solutions. This D/H exchange gives a baseline drift as a consequence. In addition, each increase in the protein concentration results in a small but not negligible variation in the protein-to-solvent ratio. This leads to a disparity in solvent concentration between the reference and the sample, causing an additional contribution to the drift of the baseline.

Protein concentrations were determined from the UV−visible spectra measured with the Shimadzu UV-2101PC spectrophotometer and using the absorption coefficients $\epsilon_{418\ nm} = 122\ mM^{-1}\ cm^{-1}$ and $\epsilon_{452\ nm} = 9.8\ mM^{-1}\ cm^{-1}$ for BMP and FMND, respectively (*26*, *31*). We scaled the first component infrared spectra to 1 mM in protein concentration with an optical path length of 23.6 μm and called them standard spectra. The infrared absorption coefficients for the amide I′ band of BMP and FMND were determined to be 179.2 ± 1.3 $mM^{-1}\ cm^{-1}$ (1653 cm^{-1}) and 69.1 ± 0.4 $mM^{-1}\ cm^{-1}$ (1638 cm^{-1}), respectively.

(ii) Spectra of the Protein Mixtures (Mixture Spectra). The spectra of the protein mixtures suffer from the same experimental errors as were discussed above. Great care was taken to work in the nitrogen-flushed glovebox and to make all necessary corrections, which included the baseline correction, the correction on the BMP absorption, and the scaling correction on the actual concentration of FMND in the sample.

To correct the baseline drift, a polynomial function was used as a complement to the linear combination of the spectral standards in the least-squares fit of the spectra of protein mixtures taken in the range of 1500−1800 cm^{-1}. It was found that only 5th and 6th polynomials give the best and very similar fitting results for the spectra in the range of 1500−1800 cm^{-1} to diminish the curve deformations at the ends of the spectra (in the ranges of 1750−1800 and 1500−1530 cm^{-1}). The preference was given to the 5th polynomial. The correcting polynomials did not show any wings within the spectral region of interest (1500−1750 cm^{-1}), which would disturb or produce difference absorption signals.

The fitting of the mixture spectra for one titration curve by the standard spectra gives a set of concentrations for both BMP ($C_{BMP,j}$) and FMND ($C_{FMND,j}$). Subtraction of the BMP standard spectrum, adjusted to the respective $C_{BMP,j}$ from each spectrum in the titration series, results in a series of the spectra that reflect only the changes in the FMND concentration overlapped with the association-induced changes in the spectra of both proteins. These spectra were then scaled to the same FMND concentration using $C_{FMND,j}$.

Principal Component Analysis (PCA). This approach is based on the analysis of a matrix **D** built from a series of spectra reflecting the course of chemical or structural transitions in the system induced by changes in concentration of the components. The matrix **D** is formed by the elements d_{ij}, where subscript i indicates the rows of the wavenumbers while j indicates the columns of the individual spectra, corresponding in our case to each of the individual titration points in the titration series or to each of the individual concentration when only the pure proteins are analyzed. In the implementation of PCA used in the present work, the matrix **D** is composed by the difference spectra obtained by subtraction of the first spectrum in the series from each subsequent one. Therefore, **D** has the dimension of $m \times (n - 1)$, where m is the number of the wavelength points in each spectrum and n is the number of the titration points in the series of protein mixtures. In the case of the PCA of the pure proteins, the first spectrum is given by a nearly zero-absorption at each wavelength ((buffer − buffer) − difference spectrum), while the pure FMND spectrum at fixed concentration forms the first spectrum for the protein mixture.

If our titration induces r independent transitions accompanied with spectral changes, the **D** matrix elements d_{ij} is considered as the sum of r products of the difference absorption coefficients e_{iq}, characterizing the qth independent

spectral transition at *i*th wavelength, and the values c_{qj} reflecting the concentration of the *q*th independent spectral component at each *j*th titration point:

$$d_{ij} = \sum_{q=1}^{r} e_{iq} \cdot c_{qj} \quad (1)$$

Equation 1 is expressed in matrix form as

$$\mathbf{D} = \mathbf{E} \times \mathbf{C}^{\mathrm{T}} \quad (2)$$

where the superscript T denotes a transposed matrix of **C**.

For resolving the matrix **D** into the matrixes **E** and **C**, the technique of choice is singular value decomposition algorithm, where the matrix **D** is transformed into two matrixes composed from column and row eigenvectors, **U** and **V**, and a diagonal matrix **S**, holding the singular values

$$\mathbf{D} = \mathbf{U} \times \mathbf{S} \times \mathbf{V}^{\mathrm{T}} \quad (3)$$

Matrixes **U** and **V** are orthogonal, with the columns ordered from the most to the least significant eigenvectors. **S** is a diagonal matrix of the singular values. In the absence of experimental errors (noise), there will be *r* (number of components) positive singular values; all the other ones are zero. In practice however, when noise affects the experimental data, all singular values are positive nonzero values, which decrease with increasing component number. One of multiple possible solutions of eq 2 is given by

$$\mathbf{E} = \mathbf{U} \times \mathbf{S}; \qquad \mathbf{C} = \mathbf{V} \quad (4)$$

In general, however, this straightforward solution has no physical meaning, and the difference spectra of individual transitions are represented by the linear combinations of the rows of matrix **E**, rather then by these rows themselves. To transform eq 4 into the only physically relevant solution of eq 3, some additional information on the behavior of the system (such as the stoichiometry of the reactions, shape of the titration curves, etc.) is required. Several different techniques were introduced to implement this additional information in the transform (*15*−*18*). However, these techniques are not required in the case where $r = 1$, i.e., if there is only one physically relevant transition reflected in the spectral series. In this case the solution given by eq 4 is the only possible one. Our approach used in this work is based on the above simplification. Here we use the PCA algorithm to improve the signal-to-noise ratio in the FTIR titration series, treating the first principal component of the solution of eq 4 as the only spectral transition caused by protein−protein interactions. The validity of this approach was confirmed by the analysis of the plots of the loading factors of the first five principal components. The principal component analysis was performed using our SpectraLab software package which was described elsewhere (*19*).

Secondary Structure Analysis of the Standard Spectra of Pure Proteins. Protein secondary structure analysis was performed as described previously (*32*). Amino acid side chain infrared standard spectra for both heme- and FMN-containing domains were constructed from absorption spectra of Asp, Glu, Asn, Gln, Tyr, Arg, and His at appropriate concentrations. Glu, Asn, and Gln absolute spectra of different side chain protonation states were obtained using extinction coefficients published by (*33*). Asp, Arg, Tyr, and His side chain spectra were extracted from the infrared spectra of these amino acids measured by us at different pD (at 25 °C) and are in agreement with literature data (*9*, *33*−*35*). These spectra of the pure amino acids will be published elsewhere. The number of the amino acids considered are taken from the crystal structure data and published sequence data: for BMP, they are Asp(33), Glu(37), Asn(19), Gln(23), Tyr(12), Arg(21), and His(13); for FMND, they are Asp(17), Glu(13), Asn(11), Gln(5), Tyr(6), Arg(5), and His(4) (*27*, *30*). The spectra were subtracted from the spectral standards of pure BMP and FMND, which were then subjected to deconvolution (*10*). Deconvolution was performed with Lorentzians, a deconvolution factor of 5000 (corresponding to a Lorentz half-bandwidth of 16 cm^{-1}) and a noise reduction factor of 0.4 using the Bruker software OPUS. Curve fitting of the amino acid side chain corrected BMP, and FMND spectral standards were performed using a nonlinear least-squares curve-fit procedure using the Voigt function (convolution of a Gauss and Lorentz function) with variable Gaussian/Lorentzian ratio parameter (*36*). The number of single bands and their start values for band position needed for the fit of the amide I′ spectra were taken from the second-derivative spectra and from literature data on the secondary structure absorption band assignment (*6*, *37*). The percentage content of the specific secondary structure elements was estimated from the relative area of the corresponding bands. The single band parameters resulting from the fitting of the deconvoluted spectral standard spectra were used as start parameters for fitting of the nondeconvoluted spectra of BMP and FMND. This procedure yields single bands used for the assignment of the spectral changes reflected in the amide I′ region of the first principal component spectrum (see below).

The absorption of the heme vinyl group at about 1630−1640 cm^{-1} (*38*, *39*) was neglected in the analysis of the amide I′ band in BMP because of its low intensity compared to the absorption intensity of the large number of the peptide C═O groups. The spectra of pure FMN in D_2O and D_2O−HEPES buffer were measured in a broad pD range. They do not show any pD dependent spectral changes within the region of 1500−1800 cm^{-1}. There are two broad bands at 1702 and 1640 cm^{-1} which are assigned to C═O groups. Furthermore, two sharp bands at 1549 cm^{-1}, arising from C═C and/or C═N stretching vibration mode, and at 1581 cm^{-1} (stronger band), caused by C═N stretch vibration mode (*40*−*42*), appeared (data not shown). However, these FMN cofactor absorption bands have an absolute intensity much lower than that of the amide I′ and amide II band of the FMND protein. Therefore, these bands were not considered in the correction of the amide I′ spectrum for secondary structure analysis.

Construction of Basis Spectra and Simulation of the First Principal Component Spectrum. As stated above, the spectrum of the first principal component derived from the titration series by PCA was interpreted as reflecting the changes induced by protein−protein interactions. To sort out the physically relevant spectral changes and to interpret them one needs a set of spectra, which relate to specific structural changes. These spectra we call basis spectra. The set of the basis spectra is used to build up a simulated spectrum for the first principal component spectrum. The following basis spectra of the structural components, which are presumably

involved in the BMP−FMND complex formation, were constructed: (i) difference spectra for the structural changes of COO(D) in aspartate side chains and of C-terminal groups; (ii) single amide II bands obtained from the difference between the absolute spectra of P450cam at 35 or 60 °C minus that at 20 °C; and (iii) secondary structure single bands obtained from the fitting of both BMP and FMND spectral standards.

To simulate the spectrum of the first principal component by the linear combination of the basis spectra, we have used the curve fitting procedure implemented in the Bruker OPUS software because it is capable of considering bands with negative amplitudes. However, to perform this fitting, it was necessary to redescribe the basis spectra by a band function, which is implemented in the BRUKER software (linear combination of Lorentzians and Gaussians). Voigt functions which are physically justified (*6*) and which we used for the standard spectra fitting with our own software are not implemented in OPUS. This redescription of the bands is just a mathematical procedure and has no physical meaning. The fit of the standard spectra described above revealed that the width, shape, and position of eight single bands are very similar in BMP and FMND. Therefore, for further simulation of the spectrum of the first principal component using the OPUS software, we averaged these parameters and used only the averaged bands.

In this way, a set of 18 single bands was obtained to be considered as basis spectra in the fitting of the principal component spectrum in the region of 1500−1800 cm^{-1} (12 bands for the secondary structure, 2 bands for the aspartate (COO^- and COOD forms), 2 bands for the C-terminal carboxylate (COO^- and COOD forms), and 2 bands for the amide II band (difference 20−35 °C and 20−60 °C). During the fitting all band parameters were fixed except the amplitudes. It turned out that two additional single bands (one positive band at 1597 cm^{-1} and one negative band at 1701 cm^{-1}) had to be added to the set of bands in order to achieve the best similarity between the first principal component and the theoretical difference spectrum.

RESULTS

Infrared Spectra of Heme- and FMN-Containing Domains of Cytochrome P450BM-3 (Standard Spectra). Figure 1 represents the infrared spectra of cytochrome P450BM-3 heme domain (BMP) and flavin-containing reductase domain (FMND). These spectra were obtained as the first component in the principal component analysis of a set of spectra of the pure proteins at different concentrations (50−200 μM). The first principal components for BMP and FMND reflect 99.99% and 99.88% of the total spectral changes within a set of concentrations, respectively. The first component spectra obtained were scaled to 1 mM protein concentration with an optical path length of 23.6 μm. These scaled spectra are named as standard spectra.

Infrared Spectra for the Titration of FMN-Containing Domain by BMP (Mixture Spectra). We have chosen the BMP concentration range between 30 and 200 μM and the FMND concentration at 105 μM for our FTIR titration experiments. These concentrations revealed to be optimal to maintain an amplitude of the FTIR spectra that provide a reasonable signal-to-noise ratio while also minimizing the

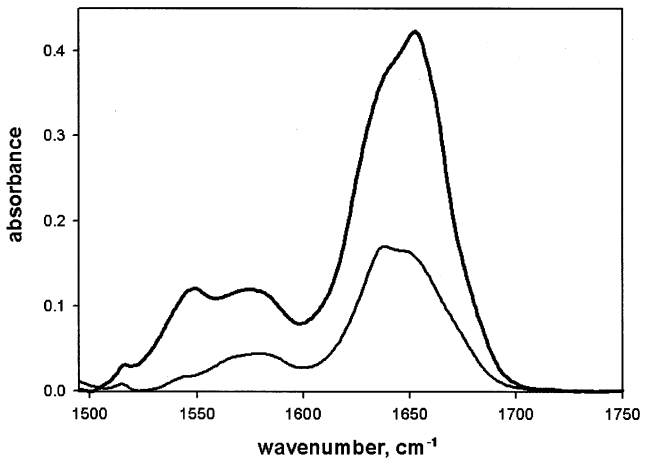

FIGURE 1: Infrared spectra of cytochrome P450BM-3 heme domain (BMP, thick line) and flavin-containing reductase domain (FMND, thin line). These spectra were obtained as the first component in the principal component analysis of a set of spectra of the pure proteins at different concentrations (50−200 μM). The spectra are scaled to a protein concentration of 1 mM each for BMP and FMND with a path length of 23.6 μM and used as standard spectra for the further analysis of the BMP−FMND complex spectra. 10 mM D_2O HEPES buffer, pD 7.4 (at 25 °C), path length 23.6 μm obtained with a Teflon spacer.

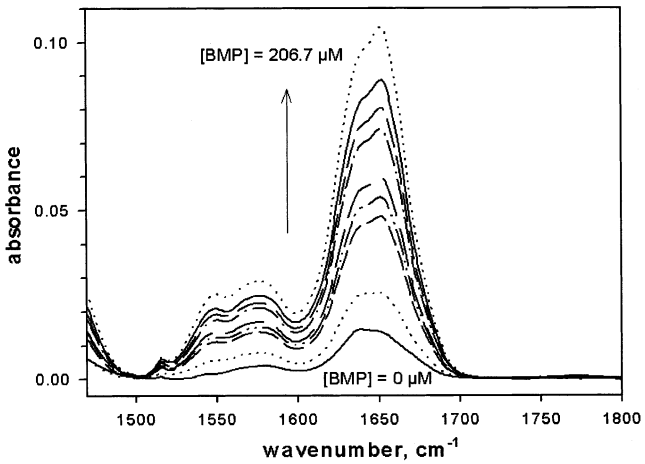

FIGURE 2: Infrared spectra of mixtures of cytochrome P450BM-3 heme domain (BMP) and flavin-containing reductase domain (FMND). The concentration of FMND was fixed at 105 μM, while the concentration of BMP was varied between 0 and 207 μM. The baseline correction was performed using least-squares fitting of the mixture spectra with a polynomial as described in Materials and Methods. 10 mM D_2O HEPES buffer, pD 7.4 (at 25 °C), path length 23.6 μm obtained with a Teflon spacer.

protein consumption. Each titration spectrum was first subjected to the baseline correction and scaling procedures, as described in Materials and Methods (Figure 2). As stated above, this pretreatment results in a series of spectra which reflect a linear combination of three terms: (i) the spectrum of FMND at fixed FMND concentration; (ii) the difference spectrum reflecting the structural changes due to the formation of the BMP−FMND complex; and (iii) some residual contribution of noise. To resolve spectrum ii, we used the principal component analysis (PCA). As stated above, our implementation of PCA deals with the difference spectra to the first spectrum in the series that is here the spectrum of FMD at the fixed concentration. The first principle component represented 76.5% of the total spectral changes within

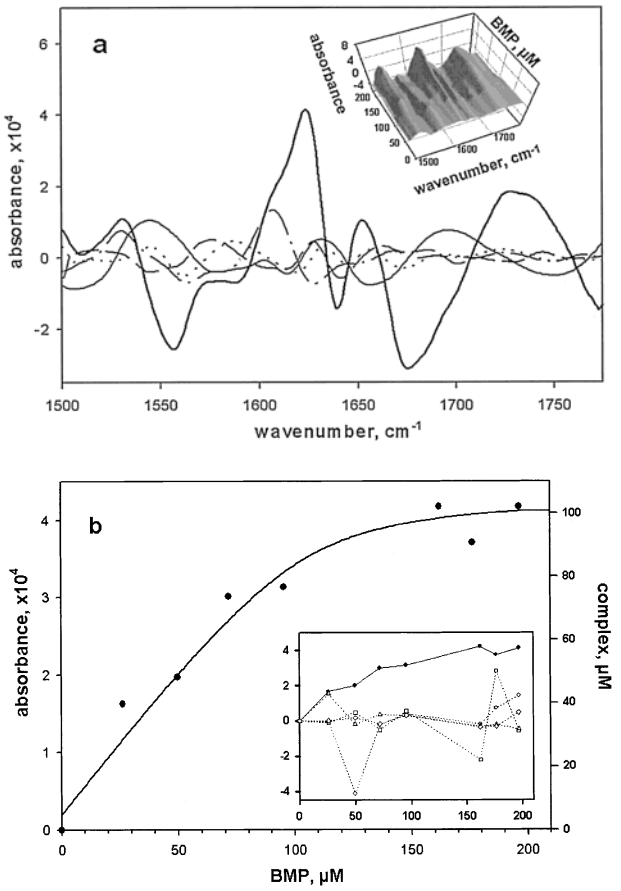

FIGURE 3: (a) The first five principal component spectra obtained by the principal component analysis of the infrared difference spectra for the mixtures of cytochrome P450BM-3 heme domain (BMP) and flavin-containing reductase domain (FMND). The difference spectra were obtained from the mixture spectra by subtracting the standard spectra of the pure proteins, scaled to the corresponding concentrations in the mixture, and by a baseline. The first principal component spectrum is smoothed with 23 point using the Savitzky−Golay algorithm and scaled using the loading factor value at the titration point of 155 μM BMP and corresponds to 100 μM concentration of the BMP−FMND complex and the optical path length of 23.6 μm. All other principal components are scaled by their respective percentage loading factors: first principal component spectrum 76.5% (thick line), second principal component spectrum 9.1% (thin line), third principal component spectrum 7.9% (dashed and dotted line), fourth principal component spectrum 2.2% (dashed line), and fifth principal component spectrum 2.1% (dotted line). The inset shows the three-dimensional view of the spectral changes at the different BMP concentrations during the titration experiment. (b) Titration curve obtained from the amplitude vector of the first principal component spectrum at the maximum at 1622 cm^{-1} vs the total BMP concentration. The dissociation constant for the BMP−FMND complex was determined by fitting of the experimental points (solid line) using the equilibrium equation for a bimolecular association BMP + FMND $\overset{K_d}{\Leftrightarrow}$ BMP·FMND; $K_d = ([BMP]\cdot[FMND])/([BMP\cdot FMND])$ with $[BMP] = [BMP]_{total} - A/A_\infty \times [FMND]_{total}$. A and A_∞ are the absorbance values at a particular BMP concentration and at infinitive concentration, respectively. A_∞ was a fit parameter besides the K_d value which revealed to be 5.1 μM. The values at the right axis represent the complex concentration calculated using the dissociation constant of 5.1 μM. Inset: overview of the amplitude vectors of the first five principal component spectra (symbols represent (●) 1st, (○) 2nd, (□) 3rd, (△) 4th, and (◇) 5th amplitude vector). Only the first amplitude vector shows a systematic dependence on the BMP concentration, while all other components do not correlate with the BMP content and must be assigned to noise.

Table 1: Amide I′ Component Bands, Relative Integrated Intensities (Population), and Secondary Structure Assignments for Heme- and FMN-Containing Domains (BMP and FMND) of Bacterial Monooxygenase Cytochrome P450BM-3 from *Bacillus megaterium*

BMP		FMND		
position, cm^{-1}	population, %	position, cm^{-1}	population, %	assignment
1609.9	4	1606.9	3	β−sheets
−	−	1617.5	4	
1622.1	3	1624.5	8	
1628.1	15	1631.2	8	
1638.2	17	1637.8	17	random coil, 3_{10}−helix
1647.4	17	1645.8	12	α−helix
1654.6	17	1651.7	8	
−	−	1657.7	8	
1663.4	18	1664.4	9	turns
1674.1	4	1672.0	23	
1680.9	5	−	−	

the series of titration spectra (Figure 3a) and was the only component that exhibited a systematic dependence on the increasing BMP concentration (Figure 3b). The fit of the experimental titration points in Figure 3b using the equilibrium equation of the bimolecular association gives a dissociation constant for the BMP−FMND complex of ∼5 μM. The shape of the titration curve confirms that the spectral changes are induced by the BMP−FMND interaction. As shown in Figure 3b (inset), the effect of noise is most pronounced at the beginning and at the end of the titration curves (i.e., at the lowest and the highest concentrations of BMP). At the initial points of the titration this originates from the low spectral amplitude due to low protein concentration, while at the last points the spectral effect is influenced by some inaccuracy in estimation of the concentration of the proteins within the fit procedure due to the small contribution of the FMND absorption in comparison to the absolute absorption of the mixture spectrum.

Analysis of the First Component Infrared Spectrum and Assignment of the Spectral Difference Signals to the Structural Changes Induced by BMP Interaction with FMND. The principal component spectrum can only be assigned to structural changes when so-called basis spectra for specific structural properties are available. The spectrum of the first principal component shown in Figure 3a reflects the spectral changes in the amide I′, amide II, and amino acid side chain absorption regions. We analyzed this infrared difference spectrum stepwise, separately for each of the three mentioned spectral regions.

Amide I′ Region. The standard spectra for the pure BMP and FMND were first corrected for amino acid side chain absorption as described (*6*, *32*), then deconvoluted and decomposed by nonlinear least-squares fit into single bands originating from the different secondary structure elements. Table 1 summarizes the band parameters, their assignment, and their population of the different secondary structure elements. The single band parameters obtained in this way were then used as an initial estimate of the parameters for the fitting of the original, nondeconvoluted side-chain corrected amide I′ bands. During this second fitting, the frequency of the bands changed only slightly, while the widths and the amplitudes changed a little bit more. These single bands finally obtained from the second fitting were

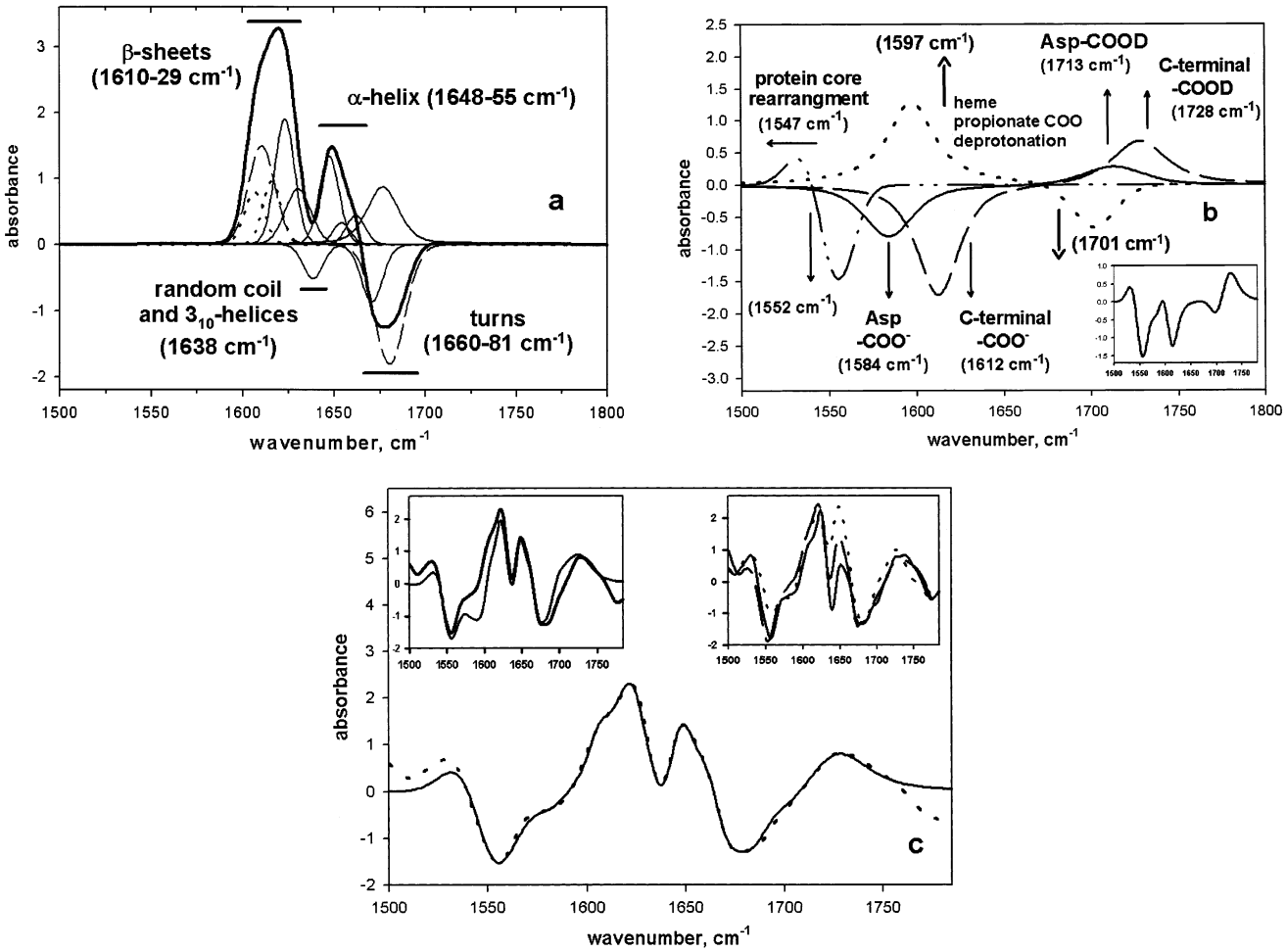

FIGURE 4: Infrared spectra of amide I′ single components of the secondary structure and difference infrared spectra reflecting the aspartate side chain protonation, amide II band change, C-terminal carboxyl group protonation, and proposed changes in heme propionate carboxyl group used for an assignment of the first principal component spectrum of the complex formation between the cytochrome P450BM-3 heme domain (BMP) and the flavin-containing reductase domain (FMND); the first principal component and theoretical difference spectrum (scaled to the BMP−FMND complex concentration of 1 mM with an optical path length of 1 cm). (a) The positive and negative bands correspond to the single bands obtained from fitting the amide I′ standard spectra of the pure proteins and belong to BMP (dashed line), FMND (dotted line), and both (solid line). The thick solid line represents the sum of all positive and negative single bands considered. (b) Difference spectra for four different structural or conformational changes except the amide I′ band which are presumably involved in the BMP−FMND complex formation. (i) Difference spectrum reflecting a protonation/deprotonation equilibrium of aspartate (solid line). This spectrum was obtained from measurements of the pure amino acid aspartate at different pD and corresponds to 1 mM aspartate and an optical path length of 1 cm. (ii) Difference spectrum reflecting a protonation/deprotonation equilibrium of a C-terminal carboxylate group (dashed line). This spectrum was extracted from spectra of different amino acids at low and high pD. Here, the spectrum of 2 mM alanine (optical path length 1 cm) is shown. (iii) Proposed difference spectrum reflecting a protonation/deprotonation equilibrium of the heme propionate carboxylate group (dotted line). This spectrum was obtained on the basis of the first principal component fitting result (see Materials and Methods and Discussion). (iv) Change of a peptide backbone N−H environment in the protein core reflected in a shift of the amide II band, resulting in a S-shape difference spectrum (dashed and dotted line). The spectrum is composed of the single bands at 1552 and 1547 cm^{-1} which were reconstructed from infrared spectra obtained in thermal unfolding experiments on cytochrome P450cam (32) and correspond to the difference of the spectra at 35 and 60 °C to 20 °C, respectively. The inset shows the sum of all represented difference spectra. The amplitudes of the single bands for the compositions shown in panels a and b were obtained from the fitting of the first principal component spectrum (Figure 3a), as described in Materials and Methods whereby band positions and widths have been fixed. (c) Overlay of the first principal component spectrum (full thick line), obtained by averaging the first principal component spectra of the three independent experiments shown in the right inset, with the sum of the theoretical basis spectra for structural changes for the amide I′ band (secondary structure) region (Figure 4a), the changes in the peptide backbone N−H environment in the protein core (amide II band), the spectral changes of the protonation state equilibrium of heme propionate and two C-terminal carboxylate groups, and the spectral change of the aspartate protonation state (Figure 4b) (dotted line). If the change in heme propionate group is not considered, then the spectrum drawn with the thin line in the left inset is obtained. The experimental first principal component is also shown in the left inset (full thick line).

used to simulate the difference infrared spectrum of the first principal component. Only the amplitude of the single bands was allowed to vary (see Materials and Methods). The result of such simulation in the amide I′ region is represented in Figure 4a. The single bands shown by dashed and dotted lines belong to BMP and FMND, respectively. The bands, which could not be differentiated between BMP and FMND because of coincidence of their maxima, are represented by thin solid lines and are considered only as merged bands. The result of the fitting shows a positive band for β-sheets (1610−1629 cm^{-1} region) and for α-helices (1648−1658 cm^{-1} region), indicating an increasing amount of these

secondary structure elements, while the populations of random coil and/or 3_{10}-helical (1638 cm^{-1}) and turn (1663−1680 cm^{-1}) structures appear to decrease.

Amino Acid Side Chain and C-Terminal Absorption Region. Searching for the spectral changes, which might be connected with salt link formation, we considered protonation/deprotonation difference spectra of all amino acid side chains absorbing in this spectral region (Asp, Glu, His, Tyr, Arg, Gln, and Asn). Side chain spectra of Glu, Gln, and Asn were constructed on the basis of literature data (*33*). In addition, the side chain spectra of Asp, Arg, Tyr, and His were measured at low pD (in DCl), at high pD (in KOD), and at pD ∼7 (D_2O HEPES buffer, pD 7).

It turned out that aspartate is the only possible candidate which can cause the spectral changes due to protonation of its carboxylate side chain which simulates the shape of the spectrum of the first principal component spectrum around 1584 and 1713 cm^{-1}. The difference spectrum of the protonation/deprotonation equilibrium of the aspartate side chain is represented in Figure 4b by the solid line. In addition, the broad signal between 1715 and 1740 cm^{-1} in the first component spectrum can only be explained by considering a protonation of two C-terminal carboxylates (band at 1728 cm^{-1} for, e.g., alanine) besides the aspartate signal. The number of groups involved can be estimated from the band intensity. A negative band at 1612 cm^{-1} originating from the deprotonated form of C-terminal carboxylates must therefore accompany the positive band at 1728 cm^{-1}. The infrared difference spectrum for the protonation of two C-terminal carboxylate groups is shown in Figure 4b by a dashed line.

Heme Propionate Carboxylate Group Spectral Region. The theoretical spectrum for the first principal component simulated by the set of the 18 basis bands did not adequately fit the spectral region around 1700 and 1600 cm^{-1}, and two additional bands had to be included (Figure 4b, dotted line). These additional bands at 1701 cm^{-1} (negative amplitude) and at 1597 cm^{-1} (positive amplitude) revealed the values for the shape, width, and area ratio parameters, which are very similar to the parameters of the bands reflecting a protonation/deprotonation equilibrium of C-terminal or aspartate side chain carboxylate groups. However, the position of these bands is more consistent with those of the absorption bands of the heme propionate carboxylate group in different protonation state (*43*, *44*).

Amide II Spectral Region. The first component spectrum shows a characteristic S-shape signal with a smaller and broader positive maximum around 1530 cm^{-1} and a sharp negative maximum around 1552 cm^{-1} (Figure 3a). This signal cannot be explained by amino acid side chain absorption but may be assigned to a shift of the amide II band of the peptide NH groups within the peptide core where the protons are not exchanged by deuterons during the dialysis of the proteins against D_2O buffer. The amide II band (NH bending and CN stretching) in H_2O is relatively unspecific for proteins and is found at about 1550 cm^{-1} (*45*). This band is used as a marker to follow protein unfolding induced by temperature. It exhibits major shifts down to 1538 cm^{-1} when the protein structure is loosened by temperature elevation as we observed in our studies on the thermal unfolding of P450cam (*32*). To fit the S-shape signal in the amide II region of the first principal component spectrum, we used the single band spectra with position of the maxima at 1552 cm^{-1} (cytochrome P450cam absolute spectrum at 35 °C minus spectrum at 20 °C) and at 1547 cm^{-1} (spectrum at 60 °C minus spectrum at 20 °C) obtained from the protein thermal unfolding experiment. The resulting theoretical amide II difference spectrum is shown in Figure 4b (dashed and dotted line). It turned out that the ratio of the area for both bands is close to unity (A_{1547} to A_{1552} is 1:1.4), indicating that the positive and the negative wings of the S-shape signal in the first component spectrum might mainly originate from the same structural change within the core with some extent of exchange of the core protons against solvent deuterons.

Reconstruction of the First Component Spectrum Using the Structural Basis Spectra. Having the relevant basis spectra for the specific structural properties, we may compare the sum of these basis spectra with the first component infrared spectrum (Figure 4c). For this comparison we used the first principal component spectrum averaged from three independent experiments (right inset in Figure 4c). These three spectra show the same overall shape and differ slightly only in the amplitude of the peak around 1650 cm^{-1}.

In the left inset of the Figure 4c, one can see that the correspondence between the experimental data and the theoretical difference spectrum (thin solid line), obtained from the sum of the structural changes in amide I′, C-terminal carboxylate, aspartate, and amide II is already sufficiently good to describe the overall shape of the experimental spectrum of the first principal component (thick solid line). However, the simulation of the spectral patterns around 1700 and 1600 cm^{-1} are still not adequate enough. This can be improved by considering two additional bands shown in Figure 4b with a dotted line and which presumably reflect the process of the deprotonation of the heme propionate carboxylate group (Figure 4c, thick solid line) as discussed above.

DISCUSSION

In this paper we describe a new strategy for the application of the Fourier transform infrared spectroscopy in studies of the structural changes in proteins induced by their interactions. This approach was applied to study the interaction between the heme- and FMN-containing domains of P450BM-3. Here we discuss our results concerning (i) the novel methodological approach, (ii) the secondary structure of BMP and FMND in solution, and (iii) changes in their structure induced by protein−protein interactions.

(i) A New Approach to Achieve Difference Infrared Spectra Reflecting the Formation of Protein−Protein Complexes. The combination of the FTIR-technique with the protein titration experiments and subsequent mathematical analysis of the spectral data by the principal component analysis is capable of resolving the infrared spectra reflecting the formation of the protein−protein complex. Using this approach we are able to overcome the difficulties which commonly appear when difference infrared spectra are taken from different sample loadings or when protein mixtures are studied. These difficulties are mainly induced by solvent effects, D/H exchange problems (*46*), protein concentration inaccuracies, and noise when the spectral effect is small and results from differences of large absorption bands. The

dependence of the loading factors on the experimental variable (the concentration of BMP in our experiments) might be directly used to probe whether the first principal component in fact reflects the formation of the protein complex. This approach demonstrates an unbiased way of studying protein−protein interaction and can be regarded as an essential improvement of the difference spectroscopic methods used by Holloway and Mantsch (*7*). These authors made the first FTIR study of a protein−protein complex formation between cytochrome b_5 and cytochrome *c*. The single-beam intensity spectrum of the mixture of both proteins was set in ratio to the intensity spectrum of pure cytochrome *c*, which corresponds to the difference of the absolute absorption spectra for which the same background spectrum is used. From this so obtained difference spectrum, the cytochrome b_5 spectrum was interactively subtracted until the absorbance at 1750 and 1520 cm^{-1} became equal and was then set to zero. This procedure cannot definitely distinguish the signals reflecting the complex formation from the unspecific backside effects. Nevertheless, it is interesting to note that the positive and negative peaks in their difference spectrum appear at similar positions but with different sign and amplitude, as we found for the BMP−FMND complex. We find positive bands at 1728, 1649, 1622, and 1531 cm^{-1} and negative peaks at 1680 and 1555 cm^{-1}. They observed positive signals at 1710, 1634, and 1677 cm^{-1} and negative bands at 1650 and at 1552 cm^{-1} and assigned these changes to a salt link formation involving a glutamate and to a loss of α-helix and the appearance of β-sheet structures. This assignment is based on the peak positions, which are characteristic for the respective structural elements (*4*, *6*, *47*).

We extended the assignment method by constructing the basis spectra for specific structural changes. These standard spectra were obtained from the spectra of single amino acids in the protonated and deprotonated form, as well as from the single bands of the fitted amide I′ band. Additionally, the amide II band shifted due to thermally induced structural changes in the protein core (presumably because of loosening the protein structure), and the spectral data for the propionic acid substituents of the heme reported in the literature (*44*) were considered. The spectrum of the first principal component reflecting the formation of the protein−protein complex could be adequately simulated with a linear combination of these basis spectra.

(ii) The Secondary Structure of BMP and FMND in Solution. The amide I′ band around 1650 cm^{-1} arising from the stretching mode vibration of the C═O peptide group is decomposed into single bands and used to determine the secondary structure composition (Table 1). We assigned the individual bands to the secondary structure elements according to the literature data (*4*, *6*, *32*): in the region of 1663−1681 cm^{-1} to turns, at 1654 and 1648 cm^{-1} to α-helices, at 1638 cm^{-1} to random coil plus 3_{10}-helices, and between 1622 and 1633 cm^{-1} to β-sheets. The assignment of the bands in the 1605−1617 cm^{-1} region is not clear. Aggregated proteins show positive bands in the 1614−1622 cm^{-1} region and at about 1684 cm^{-1} arising from the formation of intermolecular antiparallel β-sheets (*32*, *37*). However, aggregation of neither BMP nor FMND was observed under our experimental conditions. In previous studies (*32*) we assigned the signal around 1611 cm^{-1} to a remaining absorption of Arg and/or Tyr side chains due to incomplete spectral compensation in the amino acid side chain correction. Because we observe this band in all proteins analyzed so far and found a strong absorption change in particular in this region in the first principal component, we conclude that the bands in the 1610−1622 cm^{-1} region may originate from the secondary structures and assign them to β-sheets. The comparison with the crystal structure, PDB code 2HPD, (*27*) and CD studies (*48*) results for the BMP domain in the following: α-helices, 34% (FTIR), 47% (CD), and 47% (crystal); turns, 27% (FTIR), 19% CD, and 26% (crystal); β-sheets, 22% (FTIR), 21% (CD), and 11% (crystal); and 3_{10}-helix + unordered structure, 17% (FTIR), 12% (CD), and 5% (only 3_{10}-helix, crystal). The data for the crystal were determined using the PROMOTIF software (*49*). For various cytochrome P450s and NO synthase, we found that the PROMOTIF program systematically underestimates the β-sheet content by a factor of 2 compared to FTIR and CD data and to a manually counting the amino acids in the crystal structure involved in β-sheet (unpublished). In addition, one must not necessarily find exactly the same secondary structure composition in the crystal and in solution as Hadden et al. (*50*) have recently demonstrated by comparative FTIR study on different proteins in crystal as well as solution forms. Thus, we note that the secondary structure content obtained by FTIR reflects qualitatively the same overall distribution as obtained by the other methods—the largest component is the α-helical structure with approximately equal content for β-sheets and turn structures.

We also estimated the population of the secondary structure elements for the FMN domain (Table 1): 28% α-helices, 32% turns, 23% β-sheets, and 17% 3_{10}-helix + unordered structure. One can see that in this case the distribution of the populations is approximately equal for all secondary structures. Because the crystal structure of the FMND itself has not been solved so far, we can compare our data only with the crystal structure of FMND in complex with BMP (*3*), which appears to be in reasonable agreement for the α-helix but reveals lower percentages for the other structure elements: 31% α-helices, 17% turns, and 13% β-sheets. The differences might be explained by the difference between the sequence length of the FMND protein used in our experiments compared to that used for the crystal structure analysis because different cloning procedures were used (*3*, *30*) and because not all amino acids at the sequence ends are resolved in the crystal structure. Secondary structure differences expected due to complex formation exist as we have shown here by FTIR, but they are quantitatively small compared to the absolute population values (see below).

(iii) The Complex Formation between BMP and FMND. The simulation of the first component spectrum indicates that the following structural changes are induced by the BMP−FMND complex formation.

(1) Changes in the Secondary Structure and Structural Rearrangements in Proteins Core. In general, it is not possible to assign the changes in the single bands related to the changes in β-sheets (except 1606−1620 cm^{-1} region), α-helix, and random coil structures specifically to BMP or FMND. Nevertheless, Figure 4a shows that the complex formation between these two domains is characterized mostly by an increase in the populations of β-sheets and α-helix and a loss in the 3_{10}-helix and/or random coil content. Simultaneously we find a decrease of turn population in the

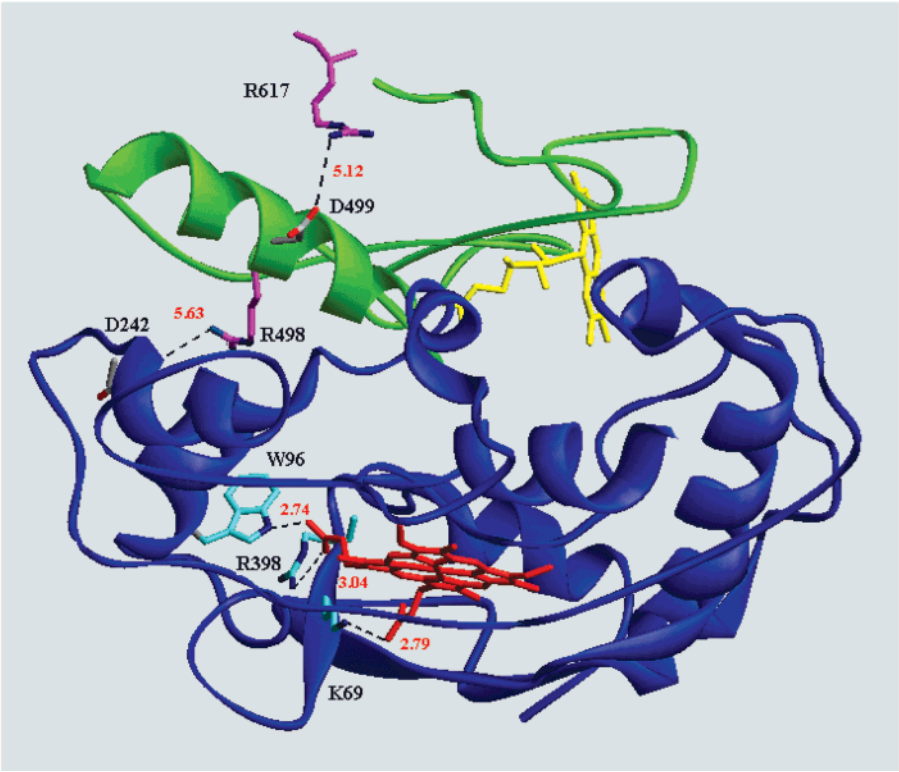

FIGURE 5: Heme−FMN domain interface. The backbones of BMP and FMND molecules are shown in blue and green, correspondingly. Aspartate and arginine side chains are shown in gray and violet, respectively. The dashed lines represent possible salt link formation between aspartate and arginine and proposed salt link cleavages between heme propionate carboxyl group and side chains of Trp96, Lys69, and Arg398, which are shown in cyan. Coordinates are taken from the crystal structure of the BMP−FMN complex (PDB code 1BVY, *3*).

BMP molecule and an increase of it in the FMND molecule. Comparing the single bands, which were possible to differentiate (Figure 4a, dashed lines for BMP and dotted lines for FMND), we note that the intensity of the spectral changes for the secondary structure in both domains is similar. However, considering that the difference in the molecular weight and therefore in the number of the relevant peptide C═O groups (the number of C═O groups in FMND is by a factor of about 2.3 smaller than that of BMP), we suppose that the changes in FMND are more pronounced. However, we hesitate to make any quantitative estimation about the extent of population change, which is quantitatively small compared to the absolute population values of the secondary structure elements. The wavenumber position of the negative and positive peaks in the difference spectrum approximately coincides with the position of the single bands for the different secondary structure elements obtained by the fitting of the standard spectra of the pure proteins. This fact gives sufficient confidence that the structural changes predominantly reflect population changes and not the band shifts, which one could also expect if the complex formation changes just the strength of the C═O bond involved in hydrogen bonding in the secondary structure element. In this case, however, S-shape difference signals with narrow peak position are expected. It also excludes that the spectral feature of the first component originates just from increase of structure ordering due to complex formation. In such cases, changes in the bandwidth of the single bands would mainly occur with unpredictable positions of negative and positive peaks in the first component spectrum.

When discussing spectral changes in the amide I′ band region, we keep in mind that the C═C stretching vibration of the vinyl group in the heme has an absorption at about 1630−1640 cm^{-1} (*38*, *39*). This contribution to the spectrum of the first principal component we ignore because of its low intensity.

The structural changes are also reflected in the amide II region (C−N stretching and N−H bending modes) that is commonly used to estimate an extent of protein folding/unfolding (*10*, *11*). In the case of the BMP−FMND complex formation, the negative amide II band at 1552 cm^{-1} is shifted toward lower frequency (down to about 1547 cm^{-1} or lower). We suppose that such behavior reflects a slight opening of the core structure of the protein accompanied with structural rearrangement within the protein core indicating a high flexibility of some regions in one or both protein molecules.

It is necessary to mention here that the weak bands from the FMN cofactor in the oxidized state appear in the spectral region of the amide II band and of the absorption region of aspartate in the deprotonated form. In HEPES buffer the band situated at 1549 cm^{-1} arises from C═C and/or C═N stretching vibration mode, and the band located at 1581 cm^{-1} is caused by C═N stretching vibration mode in FMN (*40*−*42*). These bands could contribute to the first principal component spectrum. However, we exclude this possibility because a change of the structure of the FMN isoalloxazine ring itself by FMND-BMP interaction is not expected as far as the reduction of the FMN isoalloxazine ring is avoided under our experimental conditions. In redox titration experiments, however, spectral effects can be observed in the (ox−red) difference spectrum (*41*). Moreover, the change in pD does not induce any changes in the FMN spectrum, demonstrating that the spectral contribution of FMN to the first principal component can be neglected.

(2) Protonation of a C-Terminal Carboxylate Group. We found spectral indications for a protonation change of two C-terminal COO^- groups. Although the crystal structure (*3*) does not show that the C-terminal amino acid of either BMP or FMND is located close to the interaction surface, there might be a difference in the protein domains arrangement in solution. For example, an interaction of two FMND molecules with one BMP molecule (or vice versa) would explain our finding. Indeed, Sevrioukova et al. (*51*) also concluded from reduction kinetic studies at low ionic strength that two FMND might interact with BMP. If the binding constants for both binding sites are similar, we would not be able to differentiate both these processes by the PCA procedure.

(3) Protonation of an Aspartate Carboxylate Side Chain. The change of the protonation state of the amino acid side chain groups may be an useful marker to study electrostatic inter-protein interactions as well as intramolecular salt bridge cleavage (*6*, *7*, *9*, *33*, *52*). From the X-ray data analysis (PDB code 1BVY) (*3*), it was proposed that although the interaction between FMND and BMP domains is not strong, the complex formation is mediated by two direct hydrogen bonds, one salt bridge and several water-mediated contacts. The salt link between two domains in the crystal complex is formed by His100 (BMP) and Glu494 (FMND). Because of the low infrared absorption intensity of histidine, we are unable to detect any possible changes in this residue. However, if Glu is involved in the salt link formation, the spectral changes arising from the change in the glutamate side chain protonation should be reflected in the first principal component. However, our attempt to simulate the first principal component using the spectral standard of the protonation/deprotonation difference spectrum of glutamate gave no indication that this group is involved in BMP−FMND complex formation. The only amino acid, which may be considered as a possible candidate for the electrostatic interactions, is aspartate. There is a large aspartate cluster located at FMN. It was proposed by Sevrioukova et al. that this cluster might play an important role in the interaction between the whole reductase domain and the heme domain (*3*). However, no one of these aspartates can be involved in a salt link formation with BMP so long as the Pro382-Gln387 peptide stretch, which is located in front of the FMN-containing part, does not include any positively charged amino acid residues. The only possible candidates for the salt link formation, including aspartate side chain residues, are the pairs (BMP)Asp242−(FMND)Arg498 or Asp499−Arg617 in the FMN domain (Figure 5). In the latter case, the salt link might not be formed due to the complex formation but due to a conformational change of the FMND molecule. A salt link between the FMN- and heme-domain in the second binding site for FMND discussed above might also be considered. From our infrared spectroscopic study, we have no indication for a change in an arginine.

(4) Deprotonation of a Propionic Acid Group of the BMP Heme. We have found in the simulation of the first principal component that a change in the protonation state of the heme propionate carboxylate group contributes to the first principal component. Indeed, as it was recently proposed on the basis of the combination of the heme propionate isotope labeling, protein electrochemistry, and FTIR difference spectroscopy, the protonation of heme propionate carboxylate groups is reflected in two regions as a positive band between 1670 and 1700 cm^{-1} and as a negative band in the 1540−1620 cm^{-1} region (*43*, *44*). Therefore, we assign these signals in the first principal component spectrum to the heme propionate carboxylate group of BMP in the different protonation states. It is known from the crystal structure of the BMP (*27*) that the heme propionate COO groups are involved in the salt link formation with Trp96, Lys69, and Arg398. The same is observed in the BMP/FMND crystal complex (*3*), although the position of Arg398 is slightly changed here. However, our data indicate that at least one of these salt links seems to be cleaved when BMP interacts with FMN in solution.

In summary, we have shown that the combined approach of FTIR spectroscopy, titration experiments and principal component analysis gives information about structural changes occurring during protein−protein complex formation in solution. The differences in the structural changes seen for the BMP−FMND complex by FTIR in solution and by X-ray crystal structure analysis are not completely unexpected, as the orientation of the domains in the crystal must not necessarily match the same complex in solution. It is clear that the interacting forces between proteins in the crystal are much stronger then in solution. Thus, FTIR data obtained for the BMP−FMND complex provide additional information about the structure of the complex in solution.

ACKNOWLEDGMENT

We thank J. J. Müller (Max Delbrück Center, Berlin) for carefully reading the manuscript and helpful comments.

REFERENCES

1. Pelletier, H., and Kraut, J. (1992) *Science 258*, 1748−1755.
2. Müller, J. J., Lapko, A., Bourenkov, G., Ruckpaul, K., and Heinemann, U. (2001) *J. Biol. Chem. 276*, 2789−2789.
3. Sevrioukova, I. F., Li, H., Zhang, H., Peterson, J. A., and Poulos, T. L. (1999) *Proc. Natl. Acad. Sci. U.S.A. 96*, 1863−1868.
4. Byler, D. M., and Susi, H. (1986) *Biopolymers 25*, 469−487.
5. Arrondo, J. L., and Goni, F. M. (1999) *Prog. Biophys. Mol. Biol. 72*, 367−405.
6. Jung C. (2000) *J. Mol. Recognit. 13*, 325−51.
7. Holloway, P. W., and Mantsch, H. H. (1988) *Biochemistry 27*, 7991−7993.
8. Contzen, J., and Jung, C. (1999) *Biochemistry 38*, 16253−16260.
9. Barth, A. (2000) *Prog. Biophys. Mol. Biol. 74*, 141−173.
10. Surewicz, W. K., and Mantsch, H. H. (1996) in *Spectroscopic Methods for Determining Protein Structure in Solution*, (Havel, H. A., Ed.) pp 135−162, VCH Publishers, Inc., New York.
11. Heremans, K. (1997) in *Chemistry Under Extreme and Non-classical Conditions* (van Eldik, R., and Hubbard, C. D., Ed.), pp 515−545, Wiley, New York.
12. Zhang, M., Fabian, H., Mantsch, H. H., and Vogel, H. J. (1994) *Biochemistry 33*, 10883−10888.
13. Haris, P. I., Robillard, G. T., van Dijk, A. A., and Chapman, D. (1992) *Biochemistry 31*, 6279−6284.
14. Malinowski, E. R (1991) *Factor Analysis in Chemistry*, 2nd ed., Wiley-Interscience, New York.
15. Mason, C., Maeder, M., and Whitson, A. (2001) *Anal. Chem. 73*, 1587−1594.
16. Meinrath, G., and Lis, S. (2001) *Fresenius J. Anal. Chem. 369*, 124−133.
17. Hendler, R. W., and Shrager, R. I. (1994) *J. Biochem. Biophys. Methods 28*, 1−33.
18. Durell S. R., Lee C. H., Ross R. T., and Gross E. L. (1990) *Arch. Biochem. Biophys. 278*, 148−160.
19. Davydov, D. R., Deprez, E., Hui Bon Hua, G., Knyushko, T. V., Kuznetsova, G. P., Koen, Y. M., and Archakov, A. I. (1995) *Arch. Bioch. Bioph. 320*, 330−344.

20. Schoonjans, V., Questier, F., Guo, Q., Van der Heyden, Y., and Massart, D. L. (2001) *J. Pharm. Biomed. Anal. 24*, 613−627.
21. Lee, D. C., Haris, P. I., Chapman. D., and Mitchell, R. C. (1990) *Biochemistry 29*, 9185−9193.
22. Pribic, R. (1994) *Anal. Biochem. 223*, 26−34.
23. Stelea, S. D., Pancoska, P., Benight, A. S., and Keiderlin, T. A. (2001) *Protein Science 10*, 970−978.
24. Lewis, D. F. V. (1996) *Cytochrome P450 − Structure, Function and Mechanism*, Taylor & Francis Ltd, London.
25. Shimada, H., Nagano, S., Hori, H., and Ishimura, Y. (2001) *J. Inorg. Biochem. 83*, 255−260.
26. Sevrioukova I. F., Truan, G., and Peterson, J. A.. (1996) *Biochemistry 35*, 7528−7535.
27. Ravichandran K. G., Boddupalli, S. S., Hasemann, C. A., Peterson, J. A., and Deisenhofer, J. (1993) *Science 261*, 731−736.
28. Haines, D. C., Tomchick, D. R., Machius, M., and Peterson, J. A. (2001) *Biochemistry 40*, 13456−13465.
29. Boddupalli, S. S., Oster, T., Estabrook, R. W., and Peterson, J. A. (1992) *J. Biol. Chem. 267*, 10375−10380.
30. Haines, D., Sevrioukova, I., and Peterson, J. A. (2000) *Biochemistry 39*, 9419−9429.
31. Daff, S. N., Chapman, S. K., Turner, K. L., Holt, R. A., Govindaraj, S., Poulos, T. L., and Munro, A. W. (1997) *Biochemistry 36*, 13816−23.
32. Mouro, C., Jung, C., Bondon, A., and Simonneaux, G. (1997) *Biochemistry 36*, 8125−8134.
33. Chirgadze, Y. N., Fedorov, O. V., and Trushina, N. P. (1975) *Biopolymers 14*, 679−694.
34. Hasegawa, K., Ono, T., and Noguchi, T. (2000) *J. Phys. Chem. B 104*, 4253−4265.
35. Braiman, M. S., Briercheck, D. M., and Kriger, K. M. (1999) *J. Phys. Chem. B 103*, 4744−4750.
36. Jung, C., Hui Bon Hoa, G., Schröder, K.-L., Simon, M., and Doucet, J. P. (1992) *Biochemistry 31*, 12855−12862.
37. Neault, J. F., Benkirane, A., Malonga, H., and Tajmir-Riahi, H. A. (2001) *J. Inorg. Biochem. 86*, 603−609.
38. Spiro, T. G. (1983) in *Iron Porphyrin (Part II), Physical Bioinorganic Chemistry Series* (Lever, A. B. P., and Gray, H. B., Eds.) pp 89−159, Addison-Wesley, London.
39. Berthomieu, C., Boussac, A., Mäntele, W., Breton, J., and Nabedryk, E. (1992) *Biochemistry 31*, 11460−11471.
40. Nagy, J., Kenney, W. C., and Singer, T. P. (1978) *J. Biol. Chem. 254*, 2684−2688.
41. Hellwig, P., Scheide, D., Bungert, S., Mäntele, W., and Friedrich, T. (2000) *Biochemistry 39*, 10885−10891.
42. Ariga, K., Kamino, A., Koyano, H., and Kunitake, T. (1997) *J. Mater. Chem. 7*, 1155−1161.
43. Hellwig, P., Rost, B., Kaiser, U., Ostermeier, C., Michel, H., and Mäntele, W. (1996) *FEBS Lett. 385*, 53−57.
44. Behr, J., Hellwig, P., Mäntele, W., and Michel, H. (1998) *Biochemistry 37*, 7400−7406.
45. Brazhnikov, E. V., Chetverin, A. B., and Chirgadze, Y.N. (1978) *FEBS Lett. 363*, 125−128.
46. Rahmelow K., and Hübner W. (1997) *Appl. Spectrosc. 51*, 160−170.
47. Jongh, H. H. J., Goormaghtigh, E., and Ruysschaert, J. M. (1997) *Biochemistry 36*, 13603−13610.
48. Davydov, D. R., Ponomarev, G. V., Bobrovnikova, E. V., Jung, C., and Peterson, J. A. (1999) *6th International Conference on Methods and Applications of Fluorescence Spectroscopy*, Book of Abstracts, p 15, Paris, France.
49. Hutchinson, E. G., and Thornton, J. M. (1996) *Protein Sci. 5*, 212−220.
50. Hadden, J. M., Chapman, D., and Lee, D. C. (1995) *Biochim. Biophys. Acta 1248*, 115−122.
51. Sevrioukova, I. F., Hazzard, J. T., Tollin, G., and Poulos, T. L. (1999) *J. Biol. Chem. 274*, 36097−36106.
52. Wright, W. W., Laberge, M., and Vanderkooi, J. M. (1997) *Biochemistry 36*, 14724−14732.

BI0262505